JGR Oceans

RESEARCH ARTICLE
10.1029/2025JC023608

Multidecadal Variability of Sea Surface Height and Volume Transport in the Northwestern Pacific Marginal Seas

Ho Jin Lee[1], Young-Oh Kwon[2], Sang-Yeob Kim[3], Wonsun Park[4,5], Sen Jan[6], and Yu-Heng Tseng[6]

[1]Major of Ocean Science, Korea Maritime and Ocean University, Busan, South Korea, [2]Woods Hole Oceanographic Institution, Woods Hole, MA, USA, [3]Ocean Circulation and Climate Research Center, Korea Institute of Ocean Science and Technology, Busan, South Korea, [4]Center for Climate Physics, Institute for Basic Science, Busan, South Korea, [5]Department of Integrated Climate System Science, Pusan National University, Busan, South Korea, [6]Institute of Oceanography, National Taiwan University, Taipei, Taiwan

Key Points:

- Multidecadal sea level variability in the North Pacific marginal seas is related to wind stress curl changes in the central North Pacific
- The multidecadal variability of sea surface height is a part of internal climate variability
- The volume transport variabilities of the Tsushima Warm Current and East China Sea Kuroshio do not exhibit a direct causal relationship

Correspondence to:
H. J. Lee,
hjlee@kmou.ac.kr

Citation:
Lee, H. J., Kwon, Y.-O., Kim, S.-Y., Park, W., Jan, S., & Tseng, Y.-H. (2026). Multidecadal variability of sea surface height and volume transport in the northwestern Pacific marginal seas. *Journal of Geophysical Research: Oceans*, *131*, e2025JC023608. https://doi.org/10.1029/2025JC023608

Received 16 OCT 2025
Accepted 8 JUN 2026

Author Contributions:
Conceptualization: Ho Jin Lee, Young-Oh Kwon
Data curation: Yu-Heng Tseng
Formal analysis: Ho Jin Lee
Funding acquisition: Sang-Yeob Kim
Investigation: Ho Jin Lee
Methodology: Ho Jin Lee, Young-Oh Kwon, Wonsun Park
Resources: Wonsun Park
Software: Ho Jin Lee
Supervision: Ho Jin Lee
Validation: Ho Jin Lee
Visualization: Sang-Yeob Kim
Writing – original draft: Ho Jin Lee
Writing – review & editing: Ho Jin Lee, Young-Oh Kwon, Wonsun Park, Sen Jan, Yu-Heng Tseng

Abstract The driving mechanism for the multidecadal sea surface height (SSH) variability with a period of about 50-year in the East Sea/Japan Sea and related dynamics in the northwestern Pacific marginal seas are investigated using a multi-millennial pre-industrial control climate model simulation. The model results suggest that multidecadal variability is associated with the meridional shift of zero-wind stress curl in the central North Pacific. The SSH anomalies driven by open ocean wind stress curl anomalies propagate westward via baroclinic Rossby waves and drive an anomalous sea level setup around the Japanese Islands; this leads to variability in the Tsushima Warm Current (TWC) transport, with this linkage explicitly demonstrated using the island rule. Sea surface height anomalies propagating from the open ocean also affect the Kuroshio transport in the East China Sea by modulating the onshore side of the SSH across the Kuroshio. Although the changes in the transport of the Kuroshio and TWC have opposite responses to wind stress curl changes in the central North Pacific, their direct correlation is insignificant and weakly positive. With a multi-millennial climate model simulation, this study allows a statistically robust finding on the mechanism for the multidecadal internal variability, complementing previous studies based on short term observation and reanalysis data.

Plain Language Summary Sea level in the northwestern Pacific marginal seas, including the East Sea/Japan Sea (EJS) and East China Sea (ECS), shows fluctuations on a multi-decadal cycle. This study analyzes the multi-decadal variability in sea level for a few thousand years using a climate model. Our study found that these long-term sea level variations in the marginal seas are driven by remote wind changes over the central North Pacific. The sea level changes also cause multidecadal variability in the volume transport of the Tsushima Warm Current in the EJS and the Kuroshio in the ECS, but the two are not directly related. Therefore, this study has a significance in complementing previous research findings based on reanalysis and observational data, of which the length is not long enough, by providing an insight for long-term multidecadal variability.

1. Introduction

The global mean sea level continues to rise owing to global warming. Concurrently, regional sea level changes substantially deviate from it and vary over a broad range of timescales owing to dynamic sea level changes, including ocean responses to atmospheric forcing, that is, ocean circulation changes due to wind stress (Stammer et al., 2013). Studies using large ensemble climate model simulations have shown that dynamic sea level increases due to long-term internal climate variability are comparable to those from greenhouse gas forcing, especially in the North Pacific (Bordbar et al., 2015; Hu & Deser, 2013). For instance, Sasaki et al. (2017) reported a multidecadal sea level variability around the Japanese coast since 1900. They considered it as natural variability because it was not reproduced in the multi-model ensemble mean of the historical simulations by the Coupled Model Intercomparison Project Phase 5 models. Furthermore, the amplitude of the multidecadal variability was much greater than the long-term trend from the ensemble mean.

Sea level variations in the East Sea/Japan Sea (hereafter, EJS), which is a semi-enclosed marginal sea in the northwestern Pacific that is surrounded by the Korean Peninsula, Russia, and the Islands of Japan (Figure 1a), are known to have low-frequency variability linked to oceanic circulation in the North Pacific (Gordon & Giulivi, 2004; Kang et al., 2005; Moon & Lee, 2016). The SSH anomalies (SSHa) averaged for the EJS domain (127–141°E, 35–50°N) and Tsushima Warm Current (TWC) volume transport have exhibited a multidecadal

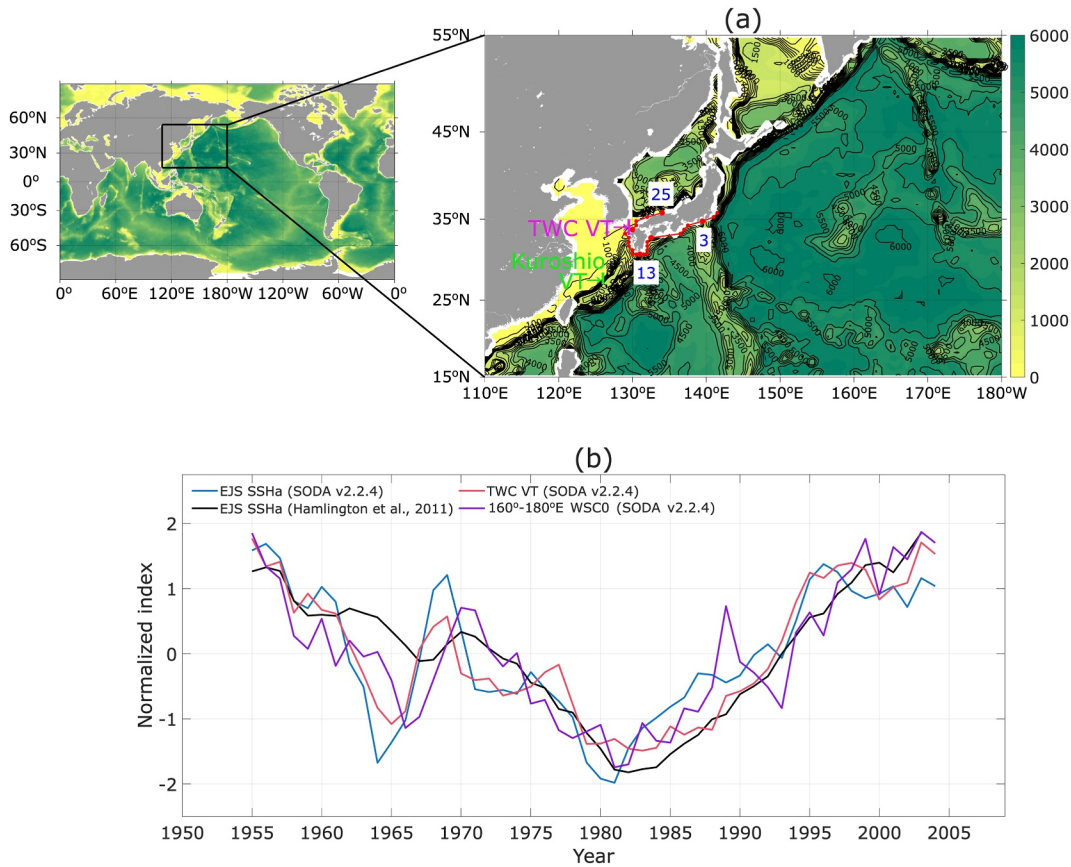

Figure 1. (a) Model domain and bathymetry with the Northwest Pacific region zoomed in. Magenta and green lines show sections where the Tsushima Warm Current (TWC) and Kuroshio volume transport are estimated, respectively. Red dots indicate coastal grid points where the monthly lag correlation is calculated in Figure 11c. (b) Time series of the domain mean sea-surface height anomalies over the East Sea/Japan Sea (EJS) region, TWC transport, and zonal mean latitude of the zero wind stress curl (WSC0) over 160°–180°E from observational and reanalysis data sets. All series are 11-year running averaged.

timescale variation, with an overall decrease until the early 1980s and an increase afterward (Figure 1b), which is consistent with the findings of Moon and Lee (2016). Notably, the zonal mean latitude of the zero-wind stress curl (hereafter, WSC0) over the central North Pacific (160–180°E) have also showed a consistent multidecadal variation with a southward WSC0 shift followed by a northward shift during the same period.

In fact, Chambers et al. (2012) had reported that there was a significant oscillation with a period around 60-year in the majority of the tide gauges examined during the 20th century. They showed recurring sea level fluctuations with an approximately 60-year period in the western North Pacific, North Atlantic and Indian Ocean (Figure 1 in Chamber et al., 2012). They stressed that the possibility of 60-year oscillation should be recognized when we interpret the acceleration in the rate of global and regional mean sea level rise although the tide gauge data still have a limitation in determining a periodic long-term fluctuation.

Gordon and Giulivi (2004) suggested that the low-frequency SSH variability in the EJS is linked to the Pacific Decadal Oscillation (PDO), which affects the strength of the Kuroshio transport in the East China Sea (ECS), which controls the throughflow into the EJS and TWC. Moon and Lee (2016) showed that the linear sea level trend in the EJS has shifted from negative (before the 1980s) to positive (after the 1980s) over the past 60 years, suggesting that such a multidecadal sea level change in the EJS is correlated with the PDO and related Kuroshio transport in the ECS, which is negatively correlated with TWC transport (Andres et al., 2009). When the Kuroshio transport in the ECS decreased (increased), the TWC transport increased (decreased), as the topographically (inertially) controlled Kuroshio jet leaked more (less) into the EJS prior to exiting the ECS through the Tokara Strait. Similarly, Shin et al. (2022) showed that the TWC transport tended to decrease from 1975 to 1988 and has

increased since the late 1980s using sea level data from the Korea Strait. Following previous studies, they reiterated that ECS Kuroshio transport changes related to the PDO drive the long-term variation in the TWC transport. However, likely because of the lack of long-term data, none of the aforementioned studies have shown a direct correlation between the TWC and Kuroshio transport in the ECS.

Kida et al. (2021) also reported a long-term (1997–2012) increasing trend in the TWC transport using sea level data for 1995–2018. However, based on a numerical simulation, they suggested that the northward shift of the Kuroshio to the south of Japan drives the increasing trend by sea level setup along the coast of Kyushu following the so-called "island rule" (Godfrey, 1989), which estimates a circulation from a sea level setup around an isolated island in response to the wind stress curl from a remote ocean. Usui and Hiorse (2025) analyzed interannual and decadal variability of the TWC transport and ocean heat transport in the EJS using a high resolution reanalysis data from 1982 to 2016. They found a close relationship between the TWC transport and sea level variability at the Japanese coast, which is explained by the propagation of coastal trapped waves (CTW) resulting from the northward migration of the Kuroshio axis around the Izu–Ogasawara Ridge (IOR).

Notably, many studies have explained the mean and seasonal cycles of TWC transport based on the island rule (Seung, 2003; Seung et al., 2012; Tsujino et al., 2008). Seung (2003) considered the bottom friction in the shallow straits of the EJS as a tuning factor to fit the observed volume transport. Seung et al. (2012) concluded that seasonal variations in volume transport in the straits of the EJS are directly controlled by remote wind-stress forcing over the North Pacific. Tsujino et al. (2008) argued that the value of the line integral of the SSH along an island in the mean state is determined by the baroclinic Rossby waves approaching the island. They also suggested that baroclinic Rossby waves are converted into baroclinic Kelvin waves and/or barotropic shelf waves after arriving at the coast and propagating along the coast and continental shelf. Yang et al. (2013) used a barotropic model to investigate the throughflow between a semi-enclosed marginal sea and a larger open ocean basin connected by channels, which is an idealized configuration of the EJS and North Pacific Ocean. They suggested that throughflow can be driven by open ocean forcing, and that horizontal friction promotes cross-isobaric flows over the ridge at the strait. Notably, these studies did not invoke a relationship with Kuroshio transport in the ECS to explain the TWC transport, suggesting that its long-term variability may not have a dynamic causality with that of the ECS Kuroshio transport. This has necessitated further investigation to determine the drivers of long-term variability in sea level in the marginal seas.

Additional driving mechanisms, including local heat/freshwater fluxes and anthropogenic aerosol forcing, have been suggested. Using a regional ocean model experiment, Sasaki et al. (2017) suggested that the recent sea level rise after 1980 was primarily caused by heat and freshwater flux forcing, while the sea level rise around 1950 was induced by wind stress curl changes over the North Pacific. Ushijima et al. (2022) argued that the decreasing sea level around the Japanese coast before 1980 came from the aerosol effect based on MRI-ESM2.0 simulation results and additional sensitivity runs. They insisted that the surface heat flux change due to the reduced shortwave radiation by aerosol radiation interaction drives sea level fall around Japan. They concluded that an increase in anthropogenic aerosols and greenhouse gases caused a decrease and increase in sea level in the North Pacific, respectively.

Therefore, whether the multidecadal variability of the SSH in the Northwest Pacific marginal seas, particularly in the EJS, is a result of natural internal variability or externally forced climate change is yet to be clarified. In this context, this study aims to examine whether multidecadal SSH variability in the EJS can be reproduced by internal variability alone and elucidate the responsible mechanisms. Because the models and observational data used in previous studies were too short to resolve the existence of multidecadal internal variability in the marginal seas around the northwestern Pacific, this study uses a 3,000-year long ocean–atmosphere coupled model to address these questions.

2. Data and Methods

2.1. Model Description

We analyzed a multi-millennial control integration with the Kiel Climate Model (KCM), a coupled atmosphere–ocean–sea ice model (Park et al., 2009). The atmospheric component, ECHAM5, has a T63 (1.875° × 1.875°) horizontal resolution with 47 vertical levels. The ocean–sea ice component, Nucleus for European Modeling of the Ocean, runs at a nominal 0.5° horizontal resolution on a curvilinear grid (ORCA05) with

46 vertical levels, including 19 levels in the upper 500 m. The version used in this study has higher atmospheric and ocean resolutions than the reference configuration described in Park et al. (2009) and shows improved performance, for example, a reduced sea surface temperature bias (not shown). Atmospheric and oceanic circulations over the North Pacific have been particularly well simulated (Choi et al., 2020; Kim et al., 2022). A list of publications on the KCM is available at https://www.geomar.de/kcms/.

The model was initialized with the observed climatology of temperature and salinity (Levitus, 1998) and run for 3,000 years under pre-industrial greenhouse gas conditions (e.g., CO_2 concentration of 286.2 ppm). We skipped the first 1,000 years to remove the initial adjustment and analyzed the annual mean values from the model run for the last 2,000 years to focus on the simulated multidecadal variability.

2.2. Data and Statistical Analysis

To examine multidecadal SSH variability, we used the 0.5° × 0.5° grid sea level data of Hamlington et al. (2011) reconstructed based on cyclo-stationary empirical orthogonal functions using both the tide gauge records for the period of 1950–2009 and satellite altimetry records during 1992–2009. Following Moon and Lee (2016), the global mean sea level trend for 1950–2009 was removed to focus on the dynamic sea level variability.

To validate the model (Section 2.3), we used current velocity and wind stress data for the same period from the Simple Ocean Data Assimilation (SODA) reanalysis, version 2.2.4, with a spatial resolution of 0.5° × 0.5° (Carton & Giese, 2008). Atmospheric forcing for SODA version 2.2.4, including wind stress, was obtained from NOAA-CIRES 20th century reanalysis version 2. The modeled SSH was validated by comparison with the C3S sea level data version DT2024, which is reprocessed delayed-time altimeter sea level data with a 0.25° resolution produced by the Copernicus Climate Change Service (Mertz et al., 2025).

The statistical significance of the linear regression coefficient was assessed using a two-tailed Student's *t*-test with an effective number of degrees of freedom (Li et al., 2013), and that of the correlation coefficient was estimated using a block bootstrap method with 1,000 resamples in blocks of 10 years (Von Storch & Zwiers, 1999). All data were analyzed after removing the linear trend at each grid point.

2.3. Model Validation

To validate the model, we first compared the monthly volume transport in the major straits of the EJS and the Kuroshio transport in the ECS with the observations (Figures 2a–2d). The KCM realistically reproduced the main characteristics of the observed TWC transport through the Korea Strait (Shin et al., 2022), including two maxima in August and October, although the means slightly differed, with 2.2 and 2.6 Sv for the KCM and observation, respectively (Figure 2a). The seasonal variation of volume transport in the Soya Strait is known to be greater than that in the Tsugaru Strait (Han et al., 2016; Oshima & Kuga, 2023; Seung et al., 2012), which is also the case in the KCM (Figures 2b and 2c). Although the model volume transport at the Tsugaru Strait (hereafter, TSVT) was smaller than the observations by approximately 0.5 Sv (Han et al., 2016), the KCM also reproduced the small annual range of the TSVT. Compared with SODA, the KCM showed much better performance in reproducing the observed volume transport of the EJS, which is likely due to the unrealistic grid configuration for the northwestern Pacific marginal seas in SODA.

The annual mean values of the Kuroshio transport in the ECS from the KCM and SODA also closely matched the observed values (Andres et al., 2008) with approximately 19 Sv. However, transport in the KCM showed a maximum in spring and a minimum in fall, whereas the observations showed a small seasonal variation of <1 Sv (Figure 2d). SODA showed a seasonal variation similar to that of KCM but with a maximum in late summer.

The modeled SSH showed a spatial distribution similar to that of the observed sea level data (Figures 2e and 2f). However, the Kuroshio Extension (KE) region was slightly diffused and shifted to the north owing to the overshooting of the Kuroshio, which is a common feature of non-eddy-resolving ocean models. The overshooting of the Kuroshio can raise the sea level on the Pacific side and reduce the volume transport, which depends on the along-channel sea level difference at the Tsugaru Strait. This explains why the modeled TSVT is smaller than the observed one.

The model showed a relatively strong wind stress curl over the open ocean and marginal seas, including the Sea of Okhotsk. However, for the WSC0 line, the model showed a distribution similar to the reanalysis data, except west

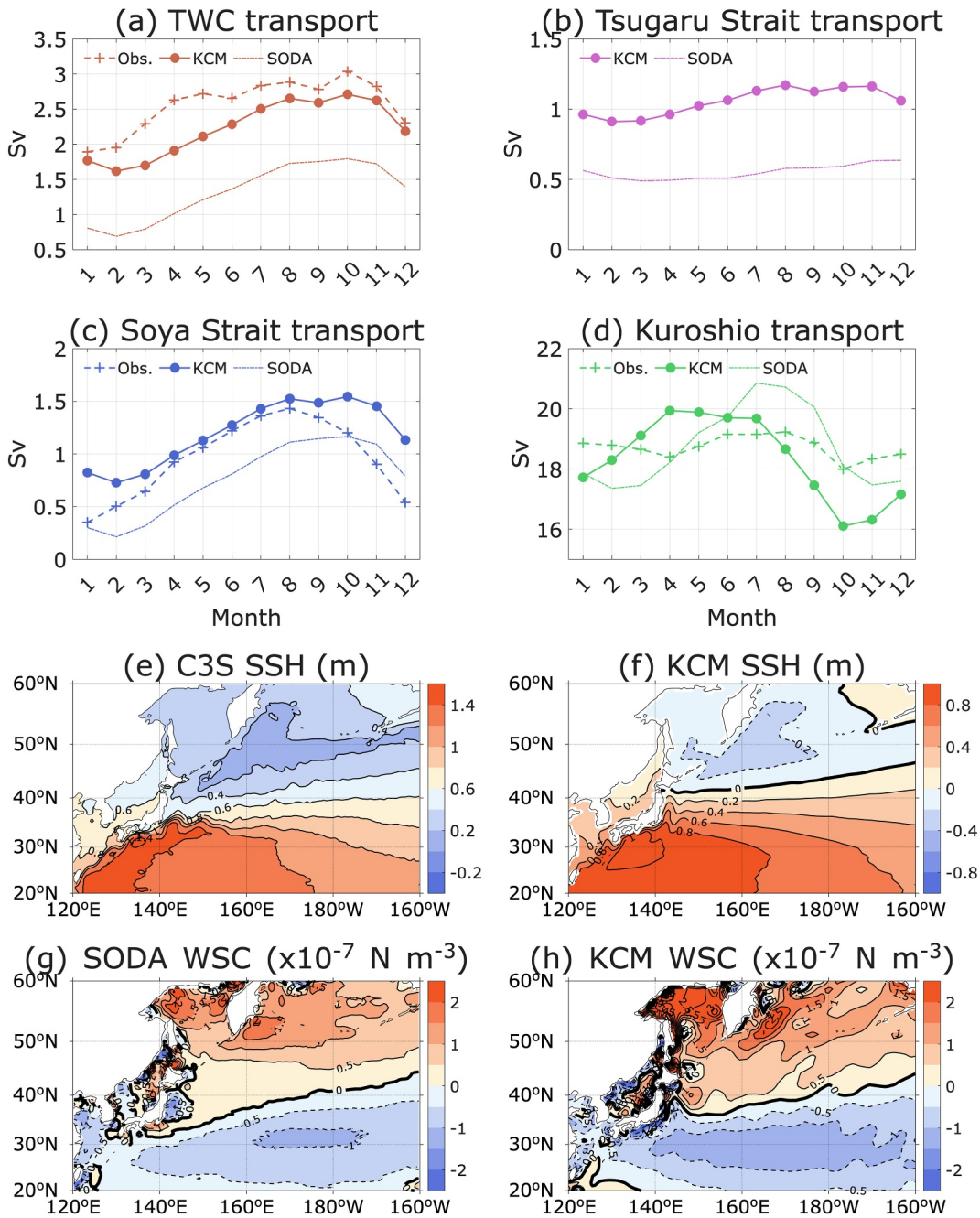

Figure 2. Climatological monthly mean volume transport of the (a) Tsushima Warm Current (TWC), (b) Tsugaru Strait, (c) Soya Strait, and (d) Kuroshio. The observed volume transports are taken from Shin et al. (2022) for the TWC, Oshima and Kuga (2023) for the Soya Strait, and Andres et al. (2008) for the Kuroshio, respectively. Time mean sea surface height (m) from (e) C3S sea level data vDT2024 for 1993–2023 and (f) Kiel climate model (KCM) for 2000 years, and wind stress curl ($\times 10^{-7}$ N/m^3) from (g) simple ocean data assimilation for 1960–2009 and (h) KCM for 2000 years.

of 150°E (Figures 2g and 2h). It is notable that the WSC0 line is tilted eastward in both SODA and KCM: 35°N near 160°E and 40°N near 180°E. Because the variability of wind stress curl can be large along the WSC0 line, we can expect wind stress curl changes between 160°E and 180°E to have a relatively high impact on coastal sea level south of the Tsugaru Strait (41°N).

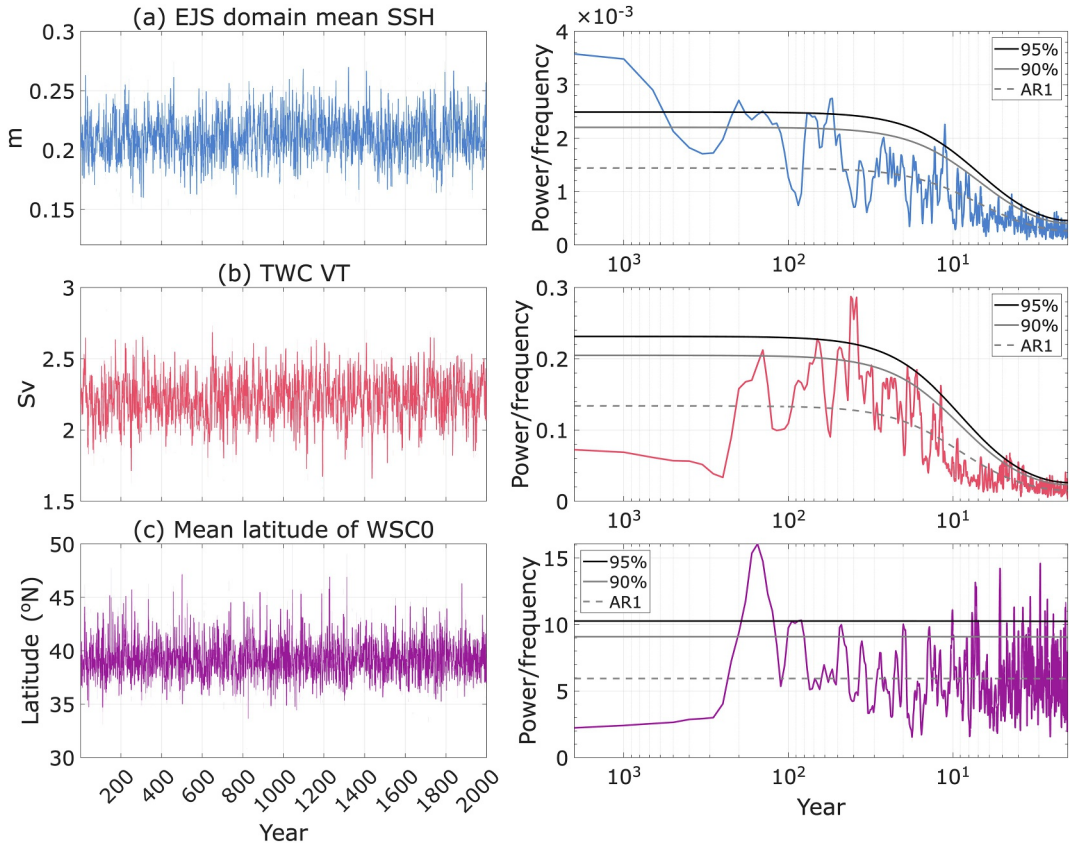

Figure 3. (a) Time series and power spectrum of the domain mean kiel climate model sea surface height anomalies over the EJS region. Black and gray solid lines indicate statistical significance at 95% and 90% for the power spectrum, respectively, while the dashed line is the red noise null hypothesis. (b)–(c) Same as (a) but for the Tsushima warm current transport and the zonal mean latitude of the WSC0 over 160°–180°E.

3. Results

3.1. Multidecadal SSH Variability and Open Ocean Wind Forcing

A spectral analysis of the EJS domain mean SSH simulated by the KCM pre-industrial control simulation was performed to confirm whether the long-term fluctuation in the observed SSH, as shown in Figure 1, could be a manifestation of internal variability with a multidecadal period. Figure 3a shows that the modeled domain mean SSH has a statistically significant peak at approximately 50–60 years. We also checked whether such a multi-decadal variability existed in the sea level of other basins (not shown). We found a statistically significant peak between 40 and 50-year periods in the North Atlantic and around 60-year periods in the Indian Ocean, while there is no statistically significant multi-decadal peak in the eastern North Pacific, which is consistent with Chambers et al. (2012). As the effect of external forcing such as global warming by greenhouse gases was not included in the KCM simulation, the reproduced multidecadal variability by the KCM can be interpreted as the internal climate variability.

The TWC transport exhibited strong peaks at approximately 40-year periods and marginally significant peaks at about 50-year (Figure 3b). The spectrum of volume transport in the Soya Strait was similar to that of the TWC transport, except without the significant peak during the 50-year period, and the spectrum of TSVT showed a peak near the 50-and 60-year periods (not shown). The mean latitude of the WSC0 showed an overall white spectrum with spectral peaks on a few multidecadal time scales, including a 50-year periodicity and a large centennial peak (Figure 3c), which will be discussed later.

An EOF analysis of the modeled SSH field was performed to examine the spatial characteristics of the low-frequency SSHa variability around the EJS (120–160°E and 25–55°N). The 2,000-year long data were

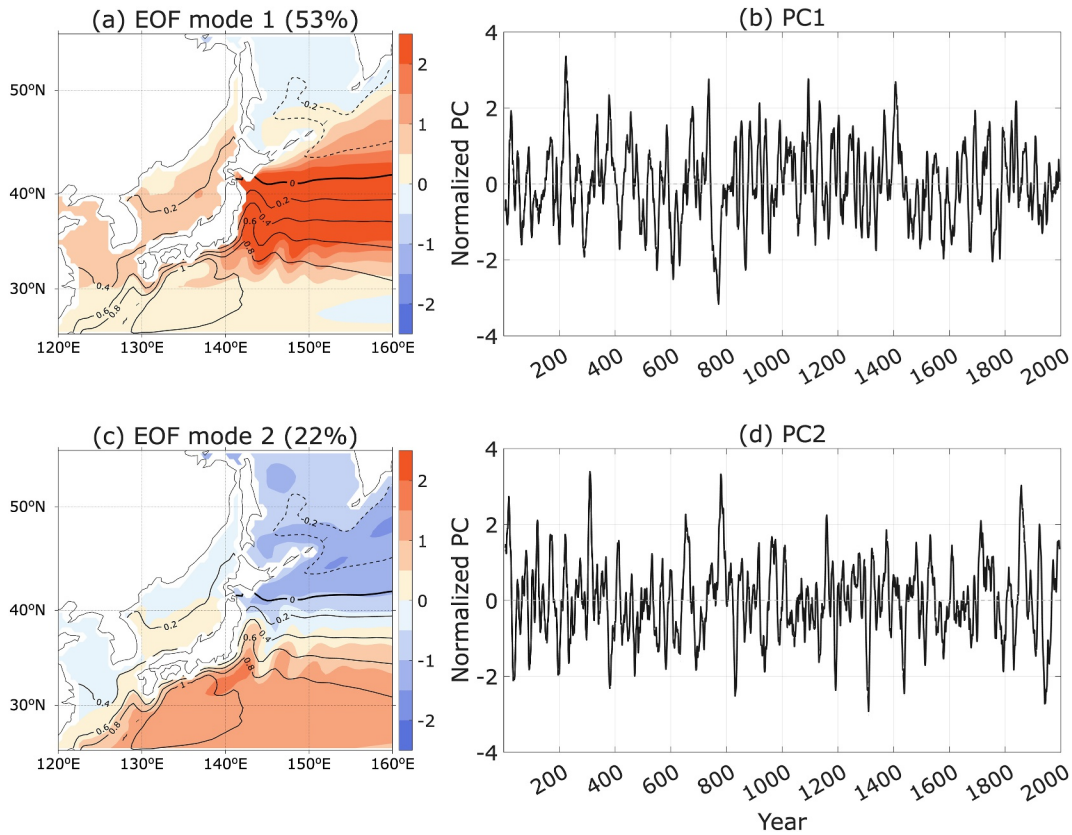

Figure 4. (a) First empirical orthogonal function (EOF) spatial pattern and (b) principal components (PC) time series of 11-year running average Kiel climate model (KCM) sea surface height anomalies in the Northwest Pacific. (c)–(d) Same as (a)–(b) but for the second EOF mode. The contours in the spatial patterns indicate the KCM 2000-year mean sea surface height. The time series are normalized by their standard deviations and the spatial patterns represent the anomalies associated with the one standard deviation fluctuation of the PC.

smoothed with an 11-year running mean prior to the EOF analysis to focus on multidecadal variation. Figure 4 shows the spatial pattern of EOF modes and associated principal components (PC), which are normalized by its standard deviation. The first EOF mode (53%) indicated a meridional shift of the subtropical gyre boundary along the Kuroshio–Oyashio Extensions and the second mode (22%) represented fluctuations in the subtropical and subpolar gyre strengths, and thereby the KE strength.

Figure 5 shows that the PC1 time series was highly correlated with the EJS mean SSHa ($r = 0.8$), as the EOF1 loading in the EJS is positive. However, the PC2 time series was statistically uncorrelated with the EJS mean SSHa, likely because of the cancellation of the positive and negative loadings in EOF2 (not shown). Therefore, we assumed that mode 1 represents the multidecadal SSHa variability in the EJS, which is directly connected to the SSHa variability in the KE region. Furthermore, the PC1 time series had a statistically significant correlation with the meridional shift of the zonal mean latitude of the WSC0 over 160°–180°E ($r = 0.7$) when the mean latitude of the WSC0 led PC1 by 1–2 years (Figure 5b). These results confirmed that long-term SSH variability in marginal seas was correlated with north–south shifts of the WSC0 in the North Pacific. Meanwhile, the PC2 time series was independent of the meridional shift of the WSC0 (not shown).

To further infer the source of SSH variability, we regressed the wind stress curl on the EJS mean SSH time series (Figure 6a). We applied an 11-year running mean to both sets of data before the regression analysis. The EJS SSH exhibited a relatively high correlation with the negative wind stress curl at approximately 40°N (160°–200°E), and the maximum correlation occurred when the wind stress curl led to 1–2 years. The maximum anomalies were near the mean WSC0, indicating that the north–south variation of the WSC0 is important for the dynamics, which is consistent with the results in Figure 5b. Given the significant multidecadal variability in the meridional shift of

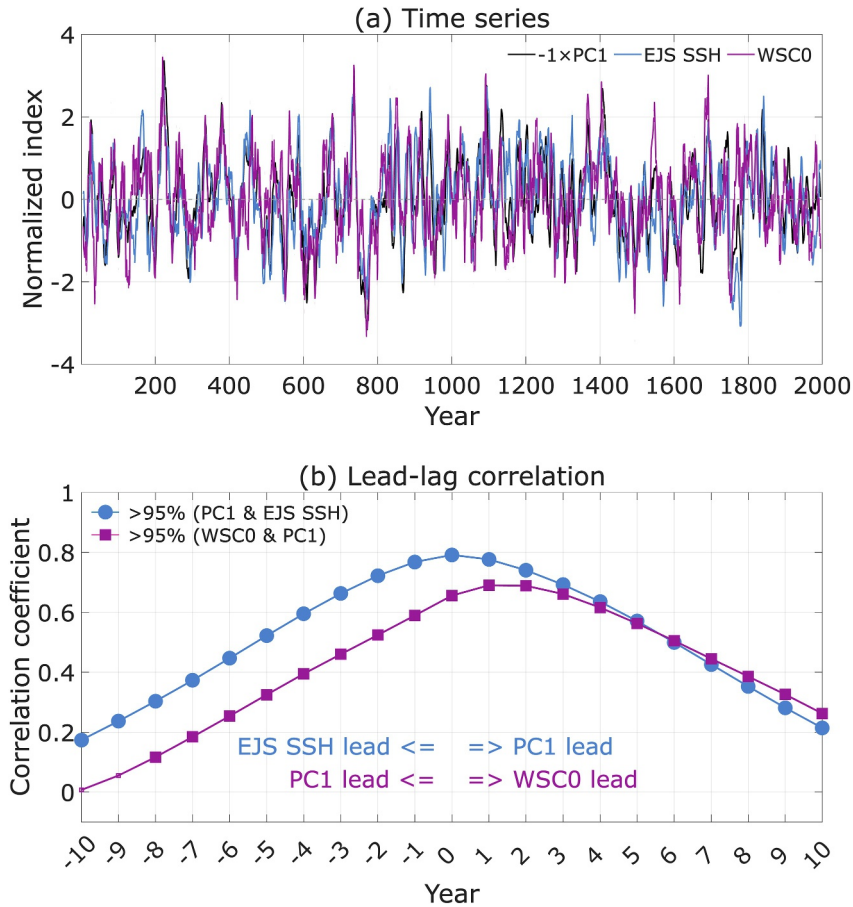

Figure 5. (a) Time series of the empirical orthogonal function PC-1 of the sea surface height anomalies (SSHa) (black), EJS mean SSHa (blue), and zonal mean latitude of the WSC0 over 160°–180°E (magenta). All the time series are based on 11-year running averaged data. (b) Lead–lag correlation between the PC-1 and EJS mean SSHa (blue), and the PC-1 and zonal mean latitude of the WSC0 over 160°–180°E (magenta). Blue circles and magenta squares indicate significant values at the 95% confidence level.

the mean latitude of the WSC0 over a 50-year period (Figure 3c), we can speculate that the EJS mean SSH with a period of approximately 50 years is associated with north–south variations in the WSC0. The positive wind stress curl anomalies near 30°N were also likely associated with the northward shift of the WSC0, given the mean wind

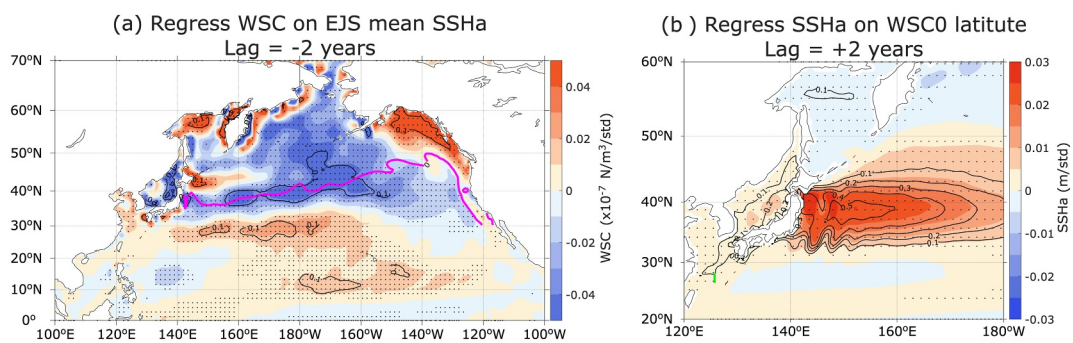

Figure 6. Regression maps of (a) wind stress curl on the EJS mean sea surface height anomalies (SSHa) and (b) SSHa on the zonal mean latitude of the WSC0 over 160°–180°E. All data are 11-year running averages. The contours and black dots indicate the explained variance (r^2) and regions with statistically significant regression coefficients at the 95% confidence level, respectively. The purple curve in (a) indicates the climatological WSC0. The green line in (b) indicates a section where the Kuroshio volume transports are estimated. A positive lag means that the time series is leading.

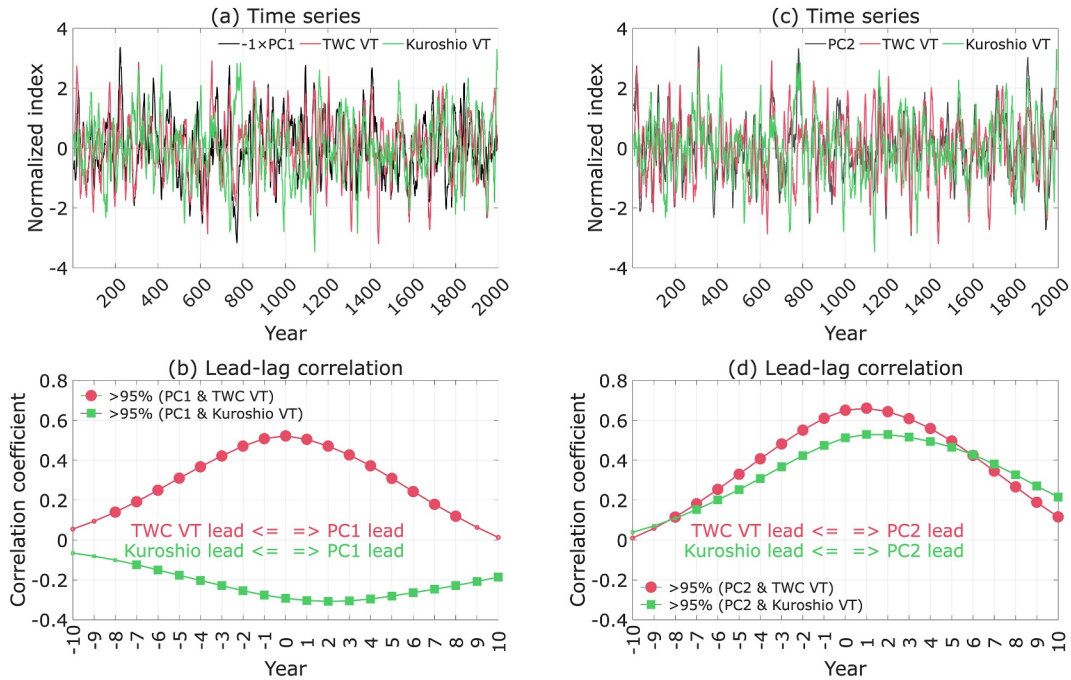

Figure 7. (a) Time series of the empirical orthogonal function PC-1 of sea surface height anomalies (black), Tsushima warm current (TWC) transport (red), and Kuroshio transport (green). All the time series are based on 11-year running averaged data. (b) Lead–lag correlation between the PC-1 and TWC transport (red), and the PC-1 and Kuroshio transport (green). (c)–(d) As in (a)–(b) but for the PC-2. Red circles and green squares in (b), (d) indicate significant values at the 95% confidence level.

stress curl pattern (Figure 2h). We also noted strong negative wind stress curl anomalies along the west coast of Japan, which may have also contributed to the increase in SSHa in the EJS.

We also regressed the SSHs on the time series of the zonal mean WSC0 to explore how the meridional shift of the WSC0 affected SSH in the marginal seas (Figure 6b). Notably, the regressed SSHa pattern was similar to that of the first EOF mode (Figure 4a), confirming that the multidecadal SSHa variability in the EJS can be related to the meridional shift of the WSC0 over the open ocean. A northward shift of the WSC0 was followed by a higher SSHa in the KE, EJS, and continental shelf in the ECS. In particular, the WSC0 had a significant impact on SSHa along the west coast of Japan. More than 20% of the multidecadal variability in the EJS off the west coast of Japan was attributed to the meridional modulation of the WSC0.

3.2. Multidecadal SSH and Volume Transport Variability

To examine the links between long-term regional sea level change and ocean circulation, we calculated the correlation between the PC time series of the SSHa (Figures 4b and 4d) and volume transport in the marginal seas. Figure 7 shows that TWC transport is positively correlated with PC1 (r = 0.5, lag = 0) and PC2 (r = 0.65, lag = 1 year), whereas the Kuroshio transport in the ECS is positively correlated with PC2 (r = 0.5) and lags by 1–2 years. This indicates that the TWC transport is directly related to the meridional shift of the KE and changes in the mean SSHa in the EJS (i.e., EOF1) as well as subtropical gyre strength variations (i.e., EOF2). Moreover, the Kuroshio transport in the ECS also increased with the subtropical gyre strength; therefore, both the Kuroshio and TWC transports were positively correlated with the strength of the subtropical gyre (Figure 7d). This result seemingly contradicts the suggestions from previous studies that the TWC transport intensity is negatively correlated with the Kuroshio transport in the ECS. Notably, the correlation coefficients between the two in the model were very low, about 0.08 and 0.07 with and without the 11-year running mean, respectively, and the TWC leads the Kuroshio by 1 year (not shown). These model results indicate that the multidecadal variability of the SSHa in the EJS can exist despite the absence of a direct link between the Kuroshio and TWC transports.

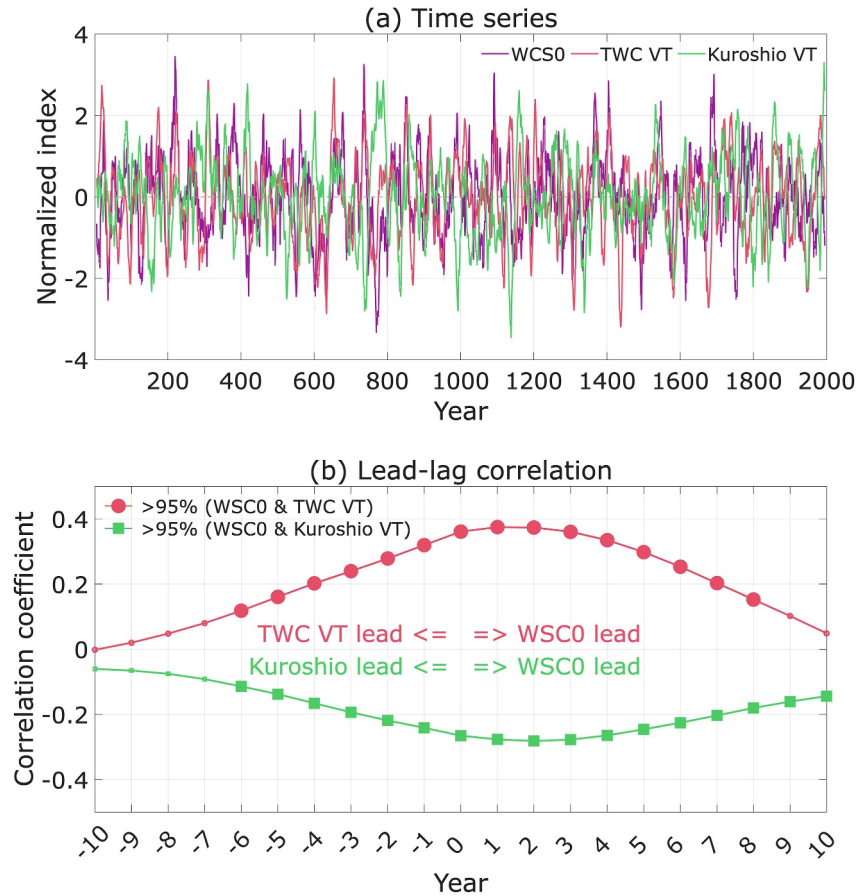

Figure 8. (a) Time series of the zonal mean latitude of the WSC0 over 160°–180°E (magenta), Tsushima warm current (TWC) transport (red), and Kuroshio transport (green). All the time series are based on 11-year running averaged data. (b) Lead–lag correlation of the zonal mean latitude of the WSC0 over 160°–180°E against TWC transport (red), and Kuroshio transport (green), respectively. Red circles and green squares indicate significant values at the 95% confidence level.

Note that the Kuroshio transport was negatively correlated with PC1 ($r \approx -0.3$) at a 1–2 years lag, although the correlation coefficient was lower than that with the TWC transport (Figure 7b). This result suggests that for multidecadal fluctuations, the wind stress curl change in the North Pacific can lead to the fluctuation of the Kuroshio transport in the ECS as well as the TWC transport, whereas the Kuroshio transport in the ECS may not necessarily drive the changes in the TWC transport. Figure 8 explicitly shows that the TWC transport has a positive correlation with the meridional shift of the zonal mean WSC0 ($r \approx 0.4$) at 1–2 years lag, whereas the Kuroshio transport has a negative maximum correlation with it ($r \approx -0.3$) at a 2 years lag. That is, the SSHa variation caused by the northward shift of the WSC0 can increase (decrease) the TWC (Kuroshio) transport, and thereby, with respect to WSC0, an inverse correlation between the two could be inferred. However, the actual correlation between the two transports was 0.08, which indicates that the Kuroshio transport is more correlated with subtropical gyre strength driven by wind stress curl south of the KE (Figure 7).

3.3. TWC Transport by Island Rule

The results thus far suggest that the multidecadal fluctuations in the TWC transport are driven by SSHa along the Japanese coast in response to the meridional variation of the WSC0 in the open ocean, instead of the changes in Kuroshio transport in the ECS. The island rule, which assumes a sea level setup around an island in response to remote changes in the wind stress curl, can be used to establish an explicit connection between the WSC0 and TWC transport.

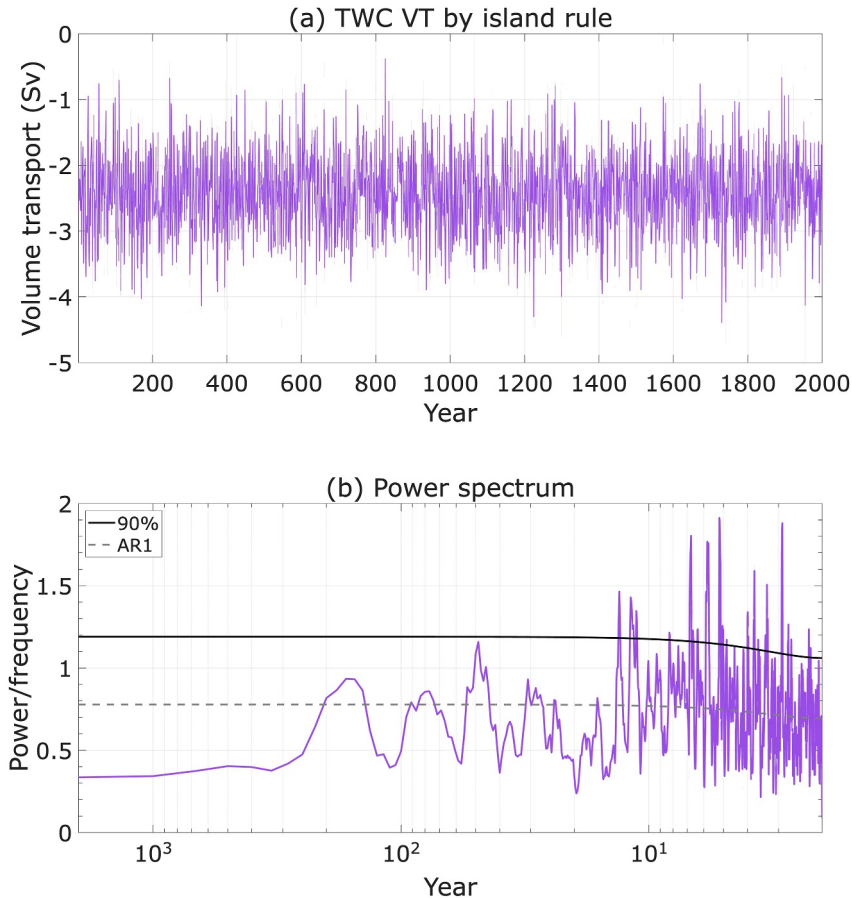

Figure 9. (a) Time series of the estimated Tsushima warm current (TWC) transport by the island rule. (b) Power spectrum of the estimated TWC transport. Solid and dashed black lines indicate statistical significance at 90% and the red noise null hypothesis, respectively.

To verify whether the multidecadal variability of the TWC transport can be explained by the island rule, we calculated the volume transports through the Korea Strait (i.e., TWC transport), Tsugaru Strait, and Soya Strait using the island rule as applied to the EJS by Seung et al. (2012). They considered a simple rectangular barotropic open ocean connecting to a marginal sea through shallow channels, which mimics the three straits of the EJS. The three channels have the same length with only along-channel flow, which is balanced with the sea level slope across the channel, and the bottom friction is balanced with the sea level slope along the channel. Zonally integrated wind stress curl drives subtropical gyre in the idealized open ocean and the circulation in the marginal sea is governed by geostrophic flows without local wind forcing.

We set the latitudinal boundary of the Japanese islands as 31.5°–41°N for Kyushu/Honshu Island, which is bounded by the Korea Strait and Tsugaru Strait to the south and north, respectively, and 41.5°–45.5°N for Hokkaido Island, which is bounded by the Tsugaru Strait and Soya Strait. We used the modeled wind stress curl over the entire zonal extent of the North Pacific (140°–240°E) and set the frictional coefficient as 0.03 s^{-1}, which is two orders larger than that in Seung et al. (2012). Note that the frictional coefficient is determined only to align the mean values of the calculated volume transport with the observed values, but the coefficients of variation, representing the ratio of the standard deviation to the mean, are constant regardless of the frictional coefficients. A detailed calculation method for this is presented by Seung et al. (2012).

Figure 9 shows the time series of the TWC transport calculated using the island rule and its power spectrum. The mean value was approximately −2.4 Sv and the standard deviation was 0.6 Sv. This negative value indicates a flow into the EJS. The mean values of volume transport in the Soya Strait and Tsugaru Strait are 1.0 and 1.4 Sv, respectively, with standard deviations of 0.5 and 0.2 Sv (not shown). Similar to the seasonal variation, the

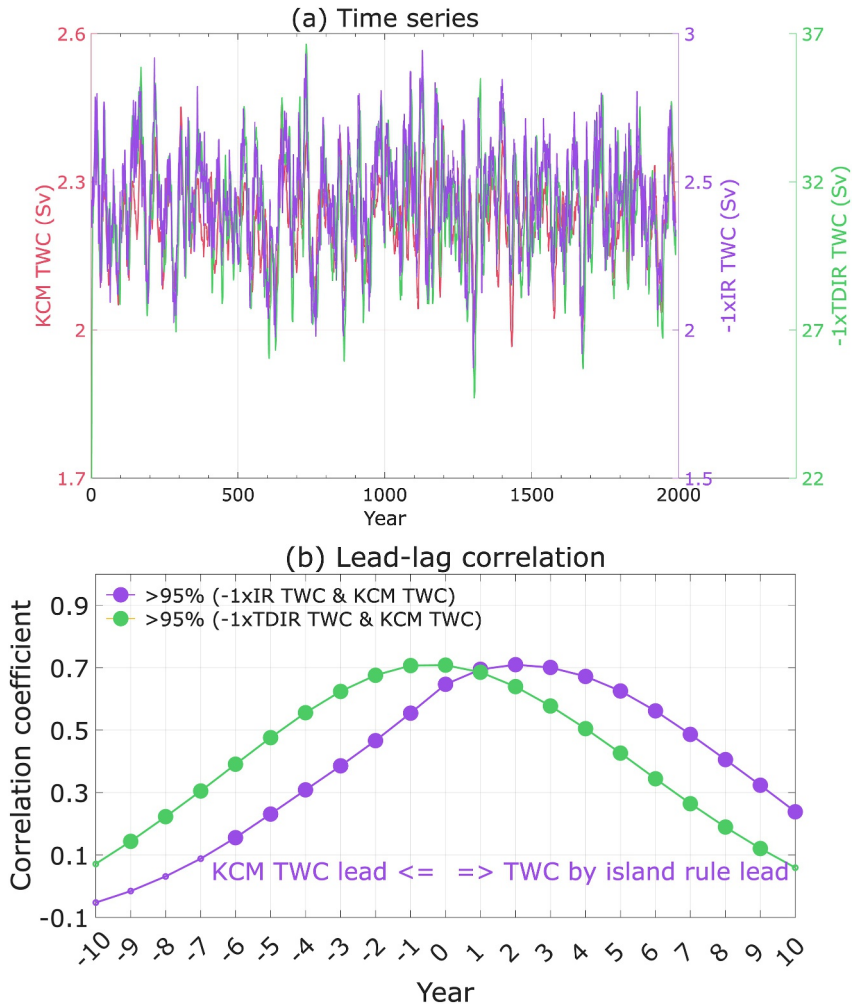

Figure 10. (a) Time series of the estimated Tsushima warm current (TWC) transport by the original island rule (IR TWC; violet) and the time-dependent island rule (TDIR TWC; green), and the TWC transport simulated by Kiel climate model (KCM) (red). (b) Lead–lag correlation between the KCM TWC transport and the island rule TWC transports. The violet and green circles indicate significant values at the 95% confidence level.

amplitude of interannual variability was smaller in the Tsugaru Strait than in the Korea Strait and Soya Strait. Although there is no statistically significant peak, but a marginally significant peak exists around 50 years. Transport in the Tsugaru Strait also had a statistically significant peak at a 50-year period (not shown).

Subsequently, we compared the calculated TWC transport by the island rule against the simulated transport by the KCM (Figure 10). The island rule TWC transport was highly correlated with the KCM TWC transport ($r = 0.7$), leading by 2 years. The lag was because the island rule calculation assumes instantaneous adjustment of the sea level to remote changes in the wind stress curl, which is not the case for the model (or the real world). Although the calculation uses wind stress curl forcing over the entire zonal extent of the North Pacific, the 2-year lag indicates that the wind stress affecting the TWC transport is mainly within the 160°–200°E longitudinal range (Figure 6a). Note that the correlation between the calculated transport and zonal mean latitude of the WSC0 over 160°–180°E was also statistically significant at approximately 0.6 with no lag (not shown). This result implies that the TWC transport can be explained by the island rule, which is described by the SSHa setup associated with remote wind stress forcing.

The conventional island rule is formulated based on the steady state solution, thus assumes an instantaneous adjustment of the sea level to remote wind changes. On the other hand, Nan et al. (2025) investigated the interannual variations of Luzon Strait Transport using a time-dependent island rule (TDIR) considering the

oceanic adjustment through baroclinic Rossby waves. Following their approach, we also calculated the TWC volume transport based on the TDIR,

$$\mathrm{TWC}_{\mathrm{TDIR}}(t) = \frac{1}{\rho_0 \left(f_N - f_S\right)} \int_{y_S}^{y_N} \int_{x_W}^{x_E} \nabla \times \tau\left(x, y, t + \frac{x_W - x}{C_R}\right) dx dy, \quad (1)$$

where x_W, x_E, y_S and y_N represent zonal (140°–240°E) and meridional (31.5°–41°N) extent; C_R is phase speed of baroclinic Rossby wave ($= -\beta g' H_1 / f^2$); H_1 is the time mean upper-layer thickness; ρ_0 is the reference density taken as 1025 kg m^{-3}; g' is the reduced gravity ($= \frac{4}{\rho_0} g$). Assuming an upper layer thickness (H_1) of 500 m, the propagation speed C_R ranges from 6.5 cm s^{-1} to 3.6 cm s^{-1} within the latitude range of 31.5° to 41°N.

It is notable that the calculated TWC transport by TDIR has the same correlation coefficient ($r = 0.7$) with the KCM TWC transport but reduces the lag to zero by explicitly incorporating the delay due to the baroclinic adjustment, which is consistent with the result by Nan et al. (2025). We emphasize that despite using the entire zonal extent wind stress curl of the North Pacific, the 2-year lag in changes confirms again that the winds affecting TWC primarily originate from the central Pacific around 180°E.

We should note that the local wind forcing over the EJS is neglected in the calculated transport by the island rule. Tsujino et al. (2008) suggested that alongshore wind induces onshore or offshore Ekman transport, generating CTW that accompany geostrophically balanced alongshore volume transport. Therefore, we can expect that the local wind stress variability, including the East Asian Monsoon, can also affect the TWC transport although it is not covered in this study.

4. Discussion

4.1. Applicability of the Island Rule

The original island rule proposed by Godfrey (1989) assumes a steady state, and lateral or bottom friction is negligible away from the western boundary. Because we applied the island rule to a time-varying aspect and invoked bottom friction, further discussion of these two aspects is warranted.

Tsujino et al. (2008) and Seung et al. (2012) applied the island rule to the mean seasonal volume transport cycle across the straits surrounding the EJS. To assume that the adjustment of the SSHa in the EJS to the wind stress curl anomalies over the North Pacific is sufficiently fast to satisfy the steady-state assumption, a barotropic adjustment should be invoked. However, Tsujino et al. (2008) suggested that the baroclinic Rossby wave was the primary mechanism, whereas Seung et al. (2012) did not provide any justification. Tsujino et al. (2008) did not show the propagation of baroclinic Rossby waves in the North Pacific open ocean because they only considered it to explain the SSHa setup in the shelf region through a transition from baroclinic Rossby waves to CTWs, which are a hybrid of internal Kelvin and barotropic shelf waves, after arriving at the east coast of Honshu.

Usui and Hiorse (2025) also showed that the propagation of CTW along the Japanese coast was responsible for TWC transport variability in the EJS. They suggested that CTW was triggered by the northward migration of the Kuroshio axis around the IOR, which was associated with the KE path; the Kuroshio around the IOR migrates northward (southward) when the KE is in a stable (unstable) state. However, whether the downstream KE affects the Kuroshio path near the IOR is debatable as some studies showed that the upstream Kuroshio meandering south of Japan is able to control the KE path and affect the Kuroshio latitudinal position (Seo et al., 2014; Wang & Tang, 2022). This topic is beyond the scope of our study and should be addressed in further study.

In our study, which concerned multidecadal SSHa variability, the first baroclinic mode Rossby wave was fast enough to justify the steady-state assumption of the island rule. Given that the SSHa setup and associated TWC transport changes in the EJS occurred in the 2 years following the wind stress curl change in the open ocean, we can assume that the SSHa in the open ocean was propagated by a baroclinic Rossby wave. To further quantify the propagation of baroclinic Rossby waves in the North Pacific, we calculated the lagged correlations of the TWC transport, wind stress curl, and SSHa at different longitudes along the latitudinal band of 32°–40°N (Figure 11). The lead–lag correlation between the modeled TWC transport and wind stress curl averaged over 32°–40°N in the KCM clearly suggested westward propagation from the central to western North Pacific (Figure 11a). The green line in Figure 11 illustrates the connection of the maximum correlation coefficients at 160°E and 180°E, where the

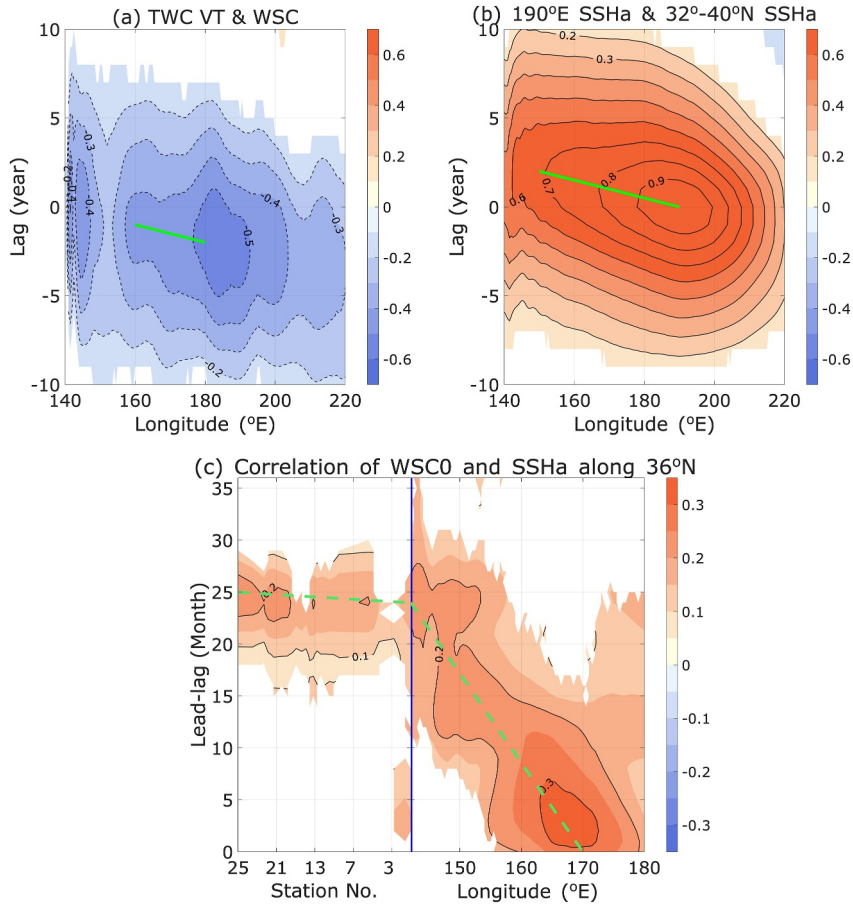

Figure 11. (a) Lead-lag correlations between the annual mean island rule Tsushima warm current transport and the meridional (32°–40°N) mean wind of stress curl at different longitudes. The green line connects the maximum correlation coefficients at 160°E and 180°E. All the time series are based on 11-year running averaged data. (b) Similar to that in (a) but with the meridional (32°–40°N) mean of sea surface height anomalies (SSHa) at 190°E and the meridional (32°–40°N) mean of SSHa at different longitudes. (c) Lead-lag correlations of the monthly zonal mean latitude of the WSC0 over 160°–180°E against the monthly mean SSHa along 36°N and the Japanese coast for model years 2800–2999. The time series are 13-month running averaged. The blue vertical line represents the boundary between the open ocean and coastal grids. The green dashed line connects the maximum correlation coefficients over the open ocean at 142°E and the boundary and over the coastal grids to the 25th coastal grid point. Color shadings show a significant correlation coefficient at the 95% confidence level.

time lag decreases from two to one year. This explains the time lag of approximately 1–2 years between the modeled TWC and zonal mean of the WSC0 (Figure 8b). The time lag between the two seemed to be skewed more toward 2 years as the maximum correlation was found at a wind stress curl around 180° (dateline). To quantify the SSHa propagation speed more directly, we also calculated the lead–lag correlation between the SSHa averaged over 32°–40°N and at 190°E for the same latitude band (Figure 11b). The SSHa appears to move at 20° longitude per year (green line), which is equivalent to a phase speed of approximately 5 cm s^{-1}. The propagation speed was slightly faster than the observational estimates in the KE region, which is 3.7 cm s^{-1} (Qiu & Chen, 2010), but consistent with the estimated baroclinic Rossby wave in climate models, for example, the Community Climate System Model version 2, in which the speed was estimated to be 2.5–7.0 cm s^{-1} in 32°–40°N (Figure 11 in Kwon & Deser, 2007).

Although the meridional averaged SSHa shows a hint of baroclinic Rossby waves propagation, it is impossible to detect SSHa moving along the Japanese coast since CTW propagates very rapidly. For that, we used a monthly data for the last 200 years to calculate a lag correlation between the zonal mean latitude of the WSC0 and the SSHa at each grid along 36°N and the Japanese coast (red dots in Figure 1b). Seasonal signal is removed by 13-month running averaged.

Figure 11c shows that a positive correlation expands westward from the central Pacific, indicating that the northward migration of WSC0 in the central Pacific induces positive SSHa due to negative wind stress curl. The phase speed calculated using the slope of the green dashed line parallel to contour lines is about 4.7 cm s^{-1}, which is consistent with the phase speed of the baroclinic Rossby wave at this latitude. It is notable that the SSHa propagate very rapidly around Honshu and Kyushu after reaching the eastern coast of Japan. Based on the propagation shown in Figure 11c (within a month), the phase speed corresponds to about 1.2 m s^{-1} (=3,000 km/(30 × 24 × 3600 s)). The typical phase speed of CTW is known to be the order of a few m s^{-1} (Tsujino et al., 2008). Although accurately examining CTW propagation is limited using monthly data, the SSHa propagation and its speed change shown in Figure 11c suggest the propagation of the baroclinic Rossby wave and conversion to CTW. According to Tsujino et al. (2008), upon arriving at the east coast of Japan, the baroclinic Rossby waves are converted into internal Kelvin waves and then into barotropic shelf waves (i.e., CTW) because they have many features in common, for example, their phase speeds are nearly the same. CTWs can propagate through the shallow strait and drive a sea level setup around Honshu and Kyushu, and thereby geostrophically balanced barotropic currents arise along the coast of Japan. Therefore, we suggest that the baroclinic mode propagating from the open ocean can be converted into the barotropic mode in the shallow continental shelf along the coast of Kyushu and Honshu, as shown in Figure 11c, which can drive the TWC transport change.

The original island rule by Godfrey (1989) did not require bottom or lateral friction because the potential vorticity (PV) contours were not blocked by shallow straits and continental shelves between the open ocean and marginal sea in their idealized flat-bottom ocean configuration. However, considering realistic topography, friction can facilitate the PV contours crossing the isobath, as argued by Yang et al. (2013), who applied the island rule by an idealized barotropic model with and without a ridge between the open ocean and marginal sea. They suggested that horizontal friction promoted cross-isobathic flows in the strait and enhanced throughflow transport. Our study used bottom friction as a factor to reduce volume transport in shallow straits and utilized it as a tuning parameter to match the observational values, following Seung (2003) and Tsujino et al. (2008). Nevertheless, the role of friction in facilitating the connection between the PV contours from the open ocean and EJS is implicit.

Chen et al. (2025) reported that the seasonal variability of the Luzon Strait Deep Overflow (LZDO) transport is largely determined by subpolar wind stress rather than by wind changes at the latitude of the Luzon Strait. They showed that the PV contours connect the Luzon Strait mainly to the subpolar North Pacific Ocean via continental slopes and suggested that the LZDO transport is connected to high latitude wind stress forcing through topographic Rossby waves propagating along the continental slope. Yang et al. (2013) also investigated the impact of the latitudinal shift in open-ocean wind forcing on the TWC transport. They, however, suggested that the remote wind forcing from the subpolar gyre is probably ineffective for the TWC because the bottom slope along the east coast of Japan, south of 35°N, is too steep, as we can see in Figure 1b.

We also estimated the PV with the model depth shown in Figure 1 (not shown). Because the depth of the Korea Strait is much shallower than that of the Luzon Strait, PV isolines in the Korea Strait are not connected to high-latitude marginal sea unlike those in the Luzon Strait. However, the PV isolines in the Okhotsk Sea and Bering Sea appear to be connected to the Soya Strait through continental shelf along the eastern coast of Sakhalin Island and Kamchatka Peninsula. To examine the impact of open-ocean wind forcing on the TWC transport, we regressed the entire North Pacific WSC on the TWC (not shown). The TWC transport was found to be correlated not only with wind stress curl at the same latitudinal range (32°–40°N) but also with that in high-latitude marginal seas, such as the Okhotsk Sea and Bering Sea. It should be noted that the high correlation with high-latitude wind forcing may not indicate a direct influence but is due to coherent fluctuation between the wind forcing along 32°–40°N and that over the high latitude marginal seas as a part of a basin scale modes of climate variability structure such as the North Pacific Oscillation. Nevertheless, it is intriguing that the area having the same background PV as the Korea Strait exhibits relatively higher correlation especially in the Okhotsk Sea.

Tsujino et al. (2008) also argued that monsoonal variation of wind stress in the Okhotsk Sea is partly responsible for the seasonal variation of the TWC and the Soya Current transports. They suggested that positive SSHa via an arrested topography wave extends to the Japan Island Chain from the Okhotsk Sea and then leads to the subsequent positive SSHa along the western boundary of the EJS and reduces TWC and the Soya Current transport in winter. We therefore cannot rule out that wind forcing in the Sea of Okhotsk or the Bering Sea also influences the multi-decadal variability of TWC transport. Furthermore, it should also be noted that the PV value itself may vary

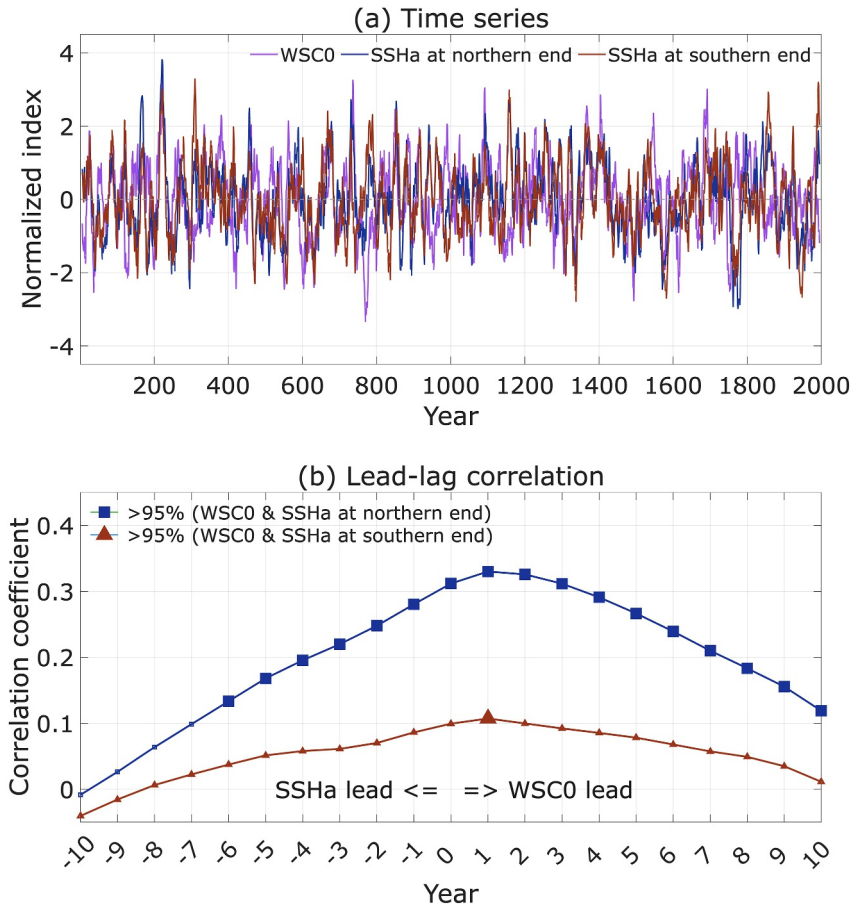

Figure 12. (a) Time series of the zonal mean latitude of the WSC0 over 160°–180°E (violet), and sea surface height anomalies (SSHa) at the northern (blue) and southern (red) end points of the green line in Figure 6b, respectively. All the time series are 11-year running averaged. (b) Lead–lag correlation of the zonal mean latitude between the WSC0 over 160°–180°Eand SSHa at the northern end point (blue), and the southern end point (red), respectively. Blue squares and red triangles indicate significant values at the 95% confidence level.

depending on the horizontal resolution of the model, which should be further addressed using high-resolution models.

4.2. Relationship Between the TWC and ECS Kuroshio Transports

As discussed in Section 1, previous studies have suggested that changes in the ECS Kuroshio transport drive the TWC transport based on apparent negative correlations from observations with limited lengths (Andres et al., 2009; Gordon & Giulivi, 2004). In contrast, our analyses of the KCM simulation did not show any significant correlation between the two at either the interannual or multidecadal timescales. Instead, our results suggest that both types of transport are driven by wind stress curl anomalies in the central North Pacific, which could explain the apparent negative correlation suggested by observational studies.

Tsujino et al. (2008) suggested that some parts of the SSHa signal along the east coast of Honshu can propagate toward low latitudes along the continental slope of the ECS, while some also travel around Kyushu and penetrate the EJS (their Figure 6). To determine whether the meridional shift of the WSC0 can drive SSH changes not only in the EJS but also on the ECS shelf to impact the Kuroshio transport, we calculated a lead–lag correlation of the zonal mean WSC0 and SSHa at the two ends of the section (green line in Figure 6b) where we estimated the Kuroshio transport in the KCM (Figure 12). The correlation was relatively higher ($r \approx 0.3$) at the northern end of the section (onshore side) than at the southern end ($r \approx 0.1$; open ocean side). These results suggest that a northward shift of the WSC0 in the North Pacific may decrease the SSH gradient across the ECS, primarily by

increasing the ECS shelf-side SSHa. Therefore, as shown in Figure 8b, the Kuroshio transport is negatively correlated with the remote WSC0 variation.

Andres et al. (2011) suggested that the Kuroshio transport in the ECS is associated with the wind stress curl around the KE, which is consistent with our findings. They showed that the interannual variability of the Kuroshio transport at the PN line, a hydrographic section crossing the Kuroshio in the ECS, is significantly correlated with the wind stress curl around 37° and 26°N, where the PN line is located. The negative (positive) wind stress curl anomalies near 37°N were associated with higher (lower) sea levels in the ECS, especially on the northern side of the PN line, thereby decreasing (increasing) volume transport in the PN line. In our study, the mean latitude of the WSC0 was located around 39°N with a standard deviation of 1.72°, which is close to the latitude of the wind stress curl anomalies (37°N) affecting the Kuroshio transport at the PN line.

Andres et al. (2011) explained the latitudinal shift of open-ocean wind forcing on the Kuroshio transport in the ECS with barotropic Rossby waves because the correlation has a zero lag with the PDO. However, they provided no clear reason for the barotropic waves crossing the Okinawa Trough, where the PN line exists. Because of the relatively short length of the data, they likely did not consider the existence of a time lag between the Kuroshio transport and wind stress curl near 37°N, although there appeared to be a time lag between the two.

4.3. TWC Transport and SSHa in the EJS

Based on the island rule, our results suggest that the TWC transport variation is driven by the SSHa in the EJS, which is triggered by open ocean wind stress curl anomalies, rather than the TWC transport change causing sea level fluctuations in the EJS, as suggested by some studies (Gordon & Giulivi, 2004; Kang et al., 2005; Moon & Lee, 2016). Kida et al. (2021) showed that the increased TWC transport in 1997–2012 was associated with a sea level trend along the coast of Kyushu (their Figure 3), although they suggested that it was caused by a north–south shift of the Kuroshio main axis south of Honshu, which in turn drove the sea level setup along the coast of Kyushu. Usui and Hiorse (2025) also showed that the positive SSHa are pronounced at the coast of Kyushu in the regression of SSHa to EOF1 of sea level along the Japanese coast, which represents the propagation of CTW (their Figure 11).

The sea level distribution in the EJS in their study is similar to the regressed SSHa pattern in Figure 6b, which is larger along the coasts of Honshu and Kyushu. Shin et al. (2022) also found that seasonal fluctuations in the TWC transport were larger in the western channel of the Korea Strait, whereas interannual and longer fluctuations were larger in the eastern channel. Moon et al. (2023) revealed an acceleration in the TWC transport after the mid-1980s using an empirical mode decomposition analysis. They also showed that the multidecadal shift mainly arose from volume transport changes in the eastern channel rather than in the western channel.

4.4. Other Potential Drivers

Sasaki et al. (2017) have suggested drivers other than open ocean wind stress forcing for the multidecadal variations of the EJS SSH, that is, heat and freshwater flux forcing. We briefly examined the relationship between the EJS mean SSHa and local net heat flux at the sea surface and found a statistically significant correlation of about −0.3 between the EJS SSHa and net heat flux (a positive value indicates heat flux from the atmosphere to the ocean), with the former leading the latter by 1 year (not shown). The correlations indicate that the increased TWC transport driven by positive EJS SSHa enhances heat transport into the EJS, and excess heat is released to the atmosphere through the sea surface.

Usui and Hiorse (2025) reported that TWC transport is a main controlling factor for the interannual variability of ocean heat content in the EJS and that the surface heat flux responds passively to the heat content changes. They showed that heat transport by the TWC leads to ocean heat content and net heat flux by about 0.5 years and 1 year, respectively. Therefore, these results are consistent with our conclusion that multidecadal SSHa variability in the EJS is primarily because of wind-driven circulation in the open ocean.

5. Summary

In this study, a multi-millennial pre-industrial control simulation using a climate model revealed a multidecadal SSH variability with a periodicity of approximately 50 years in the northwestern Pacific marginal seas. SSH variation in the EJS at an approximately 50-year time scale has also been examined in previous studies with much

shorter observations, ocean models with data assimilation, and historical simulations using coupled climate models (e.g., Moon & Lee, 2016; Sasaki et al., 2017). We found that open ocean wind stress curl anomalies associated with the meridional shift of the WSC0 in the central North Pacific drive the multidecadal variability of the SSHa, which propagates westward as baroclinic Rossby waves.

The SSHa reaching the south of Japan may propagate further along the Japanese coast by coastally trapped waves (Tsujino et al., 2008), setting up the SSHa in the EJS and changing the TWC transport, which can be explained by the island rule. The TWC transport calculated based on the island rule explained approximately 50% of the multidecadal variability in the modeled TWC transport. Therefore, we conclude that the multidecadal variability of SSH driven by the meridional shift of the WSC0 leads to the variability in the TWC transport, rather than TWC transport causing SSHa variability in the EJS.

The wind stress curl anomalies in the central North Pacific associated with the meridional shift of the WSC0 were also shown to drive the SSHa on the ECS continental shelf and Kuroshio transport by affecting the onshore side of the SSHa across the Kuroshio. Therefore, we found that the Kuroshio transport in the ECS is negatively correlated with the meridional shift of the WSC0, and the northward (southward) shift of the WSC0 drives positive (negative) SSHa over the ECS continental shelf, thus decreasing the SSH gradient across the ECS Kuroshio. Consequently, the TWC and Kuroshio transports exhibited opposite correlations to the WSC0 changes in the open ocean, suggesting an indirect negative correlation between the two. However, direct correlation between the two transports was negligible because the Kuroshio transport was more related to subtropical gyre strength.

Regarding the PDO, the SSHa EOF PC1 (Figure 4b) has a statistically significant negative correlation ($r \approx -0.8$) with the PDO (not shown), which is consistent with previous studies (Gordon & Giulivi, 2004; Moon & Lee, 2016). The mean latitude of WSC0 is also negatively correlated with PDO ($r \approx -0.5$) when the WSC0 leads PDO by 2 years (not shown). It should be noted that we consider wind stress curl as the driver of SSHa variability instead of PDO because the PDO itself is also a response to wind stress in the North Pacific.

In fact, the multi-decadal variability in the Northwest Pacific has been found in multiple climate models. Kwon and Deser (2007) have shown multi-decadal variability of about 40-year period in KE SST anomalies using a 650-year pre-industrial control integration of the Community Climate System Model version 2. Latif (2006) also showed multi-decadal variability in KE SST with a period of about 40-year using a 2,000-year long control integration of the ECHAM3/LSG CGCM. Nevertheless, we also acknowledge a need for more systematic multi-model investigation to find out whether the reproduced multi-decadal variability of SSHa is robust.

Based on our preliminary analysis, the WSC0 variability of approximately 50 years in the KCM may be related to the North Pacific Multidecadal Oscillation, which is the second mode of SST EOF in the tropical and North Pacific (120°–260°E, 20°S–60°N). Previous coupled model studies have suggested that the decadal and multi-decadal variability of the KE SST (KE dynamics) drives the North Pacific Multidecadal Oscillation (Kwon & Deser, 2007; Zhang & Delworth, 2007). The source of the decadal and multidecadal variability of the KE SST may arise within the North Pacific (Kwon & Deser, 2007) or via an inter-basin interaction originating from the Atlantic Multidecadal Oscillation (Zhang & Delworth, 2007), which should be the subject of future study.

Conflict of Interest

The authors declare no conflicts of interest relevant to this study.

Availability Statement

The C3S SSH data can be downloaded from Climate Data Source "Sea level gridded data from satellite observations for the global ocean from 1993 to present" (https://doi.org/10.24381/cds.4c328c78). The processed variables of the KCM output, the SODA reanalysis data and the Hamligton et al. (2011) data can be downloaded from https://doi.org/10.5281/zenodo.18464828.

Acknowledgments

S.-Y. Kim was supported by the in-house projects of the Korea Institute of Ocean Science and Technology (KIOST) titled "Enhancing Capacity for Assessing and Predicting Marine Environmental and Ecosystem Variability around the Korean Peninsula (PEA0403)" and the Korea Institute of Marine Science and Technology Promotion (KIMST) funded by the Ministry of Oceans and Fisheries (RS-2022-KS221667). W. Park was supported by the Korea Institute of Marine Science and Technology Promotion (KIMST) funded by the Ministry of Oceans and Fisheries, Korea (Grant RS-2023-00256330, Development of risk managing technology tackling ocean and fisheries crisis around Korean Peninsula by Kuroshio Current). The data analysis in this study was supported by the Supercomputing Center of the Korea Institute of Science and Technology Information (KISTI) with its supercomputing resources and technical support.

References

Andres, M., Kwon, Y.-O., & Yang, J. (2011). Observations of the Kuroshio's barotropic and baroclinic responses to basin wide wind forcing. *Journal of Geophysical Research*, *116*(C4), C04011. https://doi.org/10.1029/2010JC006863

Andres, M., Park, J.-H., Wimbush, M., Zhu, X.-H., Chang, K.-I., & Ichikawa, H. (2008). Study of the kuroshio/ryukyu current system based on satellite-altimeter and in situ measurements. *Journal of Oceanography*, *64*(6), 937–950. https://doi.org/10.1007/s10872-008-0077-2

Andres, M., Park, J.-H., Wimbush, M., Zhu, X.-H., Nakamura, H., Kim, K., & Chang, K.-I. (2009). Manifestation of the Pacific decadal oscillation in the kuroshio. *Geophysical Research Letters*, *36*(16), L16602. https://doi.org/10.1029/2009GL039216

Bordbar, M. H., Martin, T., Mojib, L., & Park, W. (2015). Effects of long-term variability on projections of twenty-first-century dynamic sea level. *Nature Climate Change*, *5*(4), 343–347. https://doi.org/10.1038/NCLIMATE2569

Carton, J. A., & Giese, B. S. (2008). A reanalysis of ocean climate using simple ocean data assimilation (SODA). *Monthly Weather Review*, *136*(8), 2999–3017. https://doi.org/10.1175/2007MWR1978.1

Chambers, D. P., Merrifield, M. A., & Nerem, R. S. (2012). Is there a 60-year oscillation in global mean sea level? *Geophysical Research Letters*, *39*, L18607. https://doi.org/10.1029/2012GL05288527

Chen, L., Yang, J., & Wu, L. (2025). Upstream and downstream wind-stress forcing of seasonal variability of luzon strait deep overflow transport. *Geophysical Research Letters*, *52*(1), e2024GL112817. https://doi.org/10.1029/2024GL112817

Choi, H. Y., Lee, H. J., Kim, S.-Y., & Park, W. (2020). Deepening of future aleutian low in ensemble global warming simulations with the kiel climate model. *Ocean Science Journal*, *55*(2), 219–230. https://doi.org/10.1007/s12601-020-0017-7

Godfrey, J. S. (1989). A sverdrup model of the depth-integrated flow for the world ocean allowing for island circulation. *Geophysical and Astrophysical Fluid Dynamics*, *45*(1–2), 89–112. https://doi.org/10.1080/03091928908208894

Gordon, A. L., & Giulivi, C. F. (2004). Pacific decadal oscillation and sea level in the japan/east sea. *Deep-Sea Research I: Oceanographic Research Papers*, *51*(5), 653–663. https://doi.org/10.1016/j.dsr.2004.02.005

Hamlington, B. D., Leben, R. R., Nerem, R. S., Han, W., & Kim, K.-Y. (2011). Reconstructing sea level using cyclostationary empirical orthogonal functions. *Journal of Geophysical Research*, *116*(C12), C12015. https://doi.org/10.1029/2011JC007529

Han, S., Hirose, N., Usui, N., & Miyazawa, Y. (2016). Multi-model ensemble estimation of volume transport through the straits of the east/japan sea. *Ocean Dynamics*, *66*(1), 59–76. https://doi.org/10.1007/s10236-015-0896-9

Hu, A., & Deser, C. (2013). Uncertainty in future regional sea level rise due to internal climate variability. *Geophysical Research Letters*, *40*(11), 2768–2772. https://doi.org/10.1002/grl.50531

Kang, S. K., Cherniawsky, J. Y., Foreman, M. G. G., Min, H. S., Kim, C.-H., & Kang, H.-W. (2005). Patterns of recent sea level rise in the east/japan sea from satellite altimetry in situ data. *Journal of Geophysical Research*, *110*, C07002. https://doi.org/10.1029/2004JC002565

Kida, S., Takayama, K., Sasaki, Y. N., Matsuura, H., & Hirose, N. (2021). Increasing trend in Japan sea throughflow transport. *Journal of Oceanography*, *77*(1), 145–153. https://doi.org/10.1007/s10872-020-00563-5

Kim, S.-Y., Kwon, Y.-O., Park, W., & Lee, H. J. (2022). Multidecadal regime shifts in north Pacific subtropical mode water formation in a coupled atmosphere-ocean-sea ice model. *Geophysical Research Letters*, *49*(19), e2022GL099406. https://doi.org/10.1029/2022GL099406

Kwon, Y.-O., & Deser, C. (2007). North Pacific decadal variability in the community climate system model version 2. *Journal of Climate*, *20*(11), 2416–2433. https://doi.org/10.1175/JCLI4103.1

Latif, M. (2006). On north Pacific multidecadal climate variability. *Journal of Climate*, *19*(12), 2906–2915. https://doi.org/10.1175/jcli3719.1

Levitus, S. (1998). *NODC world ocean atlas 1998 data, report, 1998*. NOAA-CIRES Clim. Diag. Cent.

Li, J., Sun, C., & Jin, F.-F. (2013). NAO implicated as a predictor of northern hemisphere mean temperature multidecadal variability. *Geophysical Research Letters*, *40*(20), 5497–5502. https://doi.org/10.1002/2013GL057877

Mertz, F., Mambert, P., & Lefèvre, F. (2025). C3S sea level vDT2024: Algorithm theoretical basis document. *E.U. Copernicus Climate Change Service*. Document ref.

Moon, J.-H., Jang, H., Kim, T., Cha, H., & Hirose, N. (2023). Non-linear long-term trend in volume transport through the korea/tsushima strait. *Frontiers in Marine Science*, *10*, 1250452. https://doi.org/10.3389/fmars.2023.1250452

Moon, J.-H., & Lee, J. (2016). Shifts in multi-decadal sea level trends in the east/Japan Sea over the past 60 years. *Ocean Science Journal*, *51*(1), 87–96. https://doi.org/10.1007/s12601-016-0008-x

Nan, F., Du, S., Yu, F., Xue, H., Li, M., & Wang, R. (2025). Revisiting the dynamics of interannual variations of the upper luzon strait transport. *Journal of Physical Oceanography*, *55*(7), 903–918. https://doi.org/10.1175/jpo-d-24-0103.1

Oshima, K., & Kuga, M. (2023). 50-year volume transport of the soya warm current estimated from the sea-level difference and its relationship with the tsushima and tsugaru warm currents. *Journal of Oceanography*, *79*(5), 499–515. https://doi.org/10.1007/s10872-023-00693-6

Park, W., Keenlyside, N., Latif, M., Ströh, A., Redler, R., Roeckner, E., & Madec, G. (2009). Tropical Pacific climate and its response to global warming in the kiel climate model. *Journal of Climate*, *22*(1), 71–92. https://doi.org/10.1175/2008jcli2261.1

Qiu, B., & Chen, S. (2010). Eddy-mean flow interaction in the decadally modulating kuroshio extension system. *Deep Sea Research II: Topical Studies in Oceanography*, *57*(13–14), 1098–1110. https://doi.org/10.1016/j.dsr2.2008.11.036

Sasaki, Y. N., Washizu, R., Yasuda, T., & Minobe, S. (2017). Sea level variability around Japan during the twentieth century simulated by a regional ocean model. *Journal of Climate*, *30*(14), 5585–5595. https://doi.org/10.1175/JCLI-D-16-0497.1

Seo, Y., Sugimoto, S., & Hanawa, K. (2014). Long-term variations of the kuroshio extension path in winter: Meridional movement and path state change. *Journal of Climate*, *27*(15), 5929–5940. https://doi.org/10.1175/JCLI-D-13-00641.1

Seung, Y. H. (2003). Significance of shallow bottom friction in the dynamics of the tsushima current. *Journal of Oceanography*, *59*(1), 113–118. https://doi.org/10.1023/A:1022828825667

Seung, Y. H., Han, S.-Y., & Lim, E.-P. (2012). Seasonal variation of volume transport through the straits of the east/japan sea viewed from the island rule. *Ocean and Polar Research*, *34*(3), 403–411. https://doi.org/10.4217/OPR.2012.34.4.403

Shin, H.-R., Lee, J.-H., Kim, C.-H., Yoon, J.-H., Hirose, N., Takikawa, T., & Cho, K. (2022). Long-term variation in volume transport of the tsushima warm current estimated from ADCP current measurement and sea level differences in the Korea/tsushima strait. *Journal of Marine Systems*, *232*, 103750. https://doi.org/10.1016/j.jmarsys.2022.103750

Stammer, D., Cazenave, A., Ponte, R. M., & Tamisiea, M. E. (2013). Causes for contemporary regional sea level changes. *Annual Review of Marine Science*, *5*(1), 21–46. https://doi.org/10.1146/annurev-marine-121211-172406

Tsujino, H., Nakano, H., & Motoi, T. (2008). Mechanism of currents through the straits of the Japan sea: Mean state and seasonal variation. *Journal of Oceanography*, *64*(1), 141–161. https://doi.org/10.1007/s10872-008-0011-7

Ushijima, Y., Tsujino, H., Sakamoto, K., Ishii, M., Koshiro, T., & Oshima, N. (2022). Effects of anthropogenic forcings on multidecadal variability of the sea level around the Japanese Coast simulated by MRI-ESM2.0 for CMIP6. *Geophysical Research Letters*, *49*(18), e2022GL099987. https://doi.org/10.1029/2022GL099987

Usui, N., & Hiorse, N. (2025). Interannual to decadal variability of ocean heat content in the Japan sea: Role of the tsushima warm current and its relation to the kuroshio extension variability. *Journal of Climate*, *38*(15), 3593–3607. https://doi.org/10.1175/JCLI-D-24-0113.1

Von Storch, H., & Zwiers, F. W. (1999). *Statistical analysis in climate research*. Cambridge University Press.494.

Wang, Q., & Tang, Y. (2022). The interannual variability of eddy kinetic energy in the Kuroshio large meander region and its relationship to the Kuroshio latitudinal position at 140°E. *Journal of Geophysical Research: Oceans*, *127*(2), e2021JC017915. https://doi.org/10.1029/2021JC017915

Yang, J., Lin, X., & Wu, D. (2013). Wind-driven exchanges between two basins: Some topographic and latitudinal effects. *Journal of Geophysical Research*, *118*(9), 4585–4599. https://doi.org/10.1002/jgrc.20333

Zhang, R., & Delworth, T. L. (2007). Impact of the Atlantic multidecadal oscillation on north Pacific climate variability. *Geophysical Research Letters*, *34*(23). https://doi.org/10.1029/2007GL031601